Progress In Electromagnetics Research Letters, Vol. 71, 141–147, 2017

Graphene-Based THz Tunable Bandstop Filter with Constant Absolute Bandwidth

Mengdan Kong*, Yongle Wu, Zheng Zhuang, Weimin Wang, and Yuanan Liu

Abstract—In this paper, a novel terahertz tunable bandstop filter with constant absolute bandwidth is proposed, which consists of graphene-based three-section L resonators. In order to perform bandstop property, the L resonator is used and analyzed in details based on the traditional Z matrix and $ABCD$ matrix. With the introduction of graphene materials, the operating frequency of bandstop filter can be extended to terahertz. Moreover, the tunable performance with constant absolute bandwidth can be achieved by only loading different chemical potentials on a graphene surface. For demonstration, a terahertz tunable bandstop filter prototype is designed and simulated with chemical potentials of 0.1, 0.3, and 1 eV. The simulated results agree well with the anticipation perfectly.

1. INTRODUCTION

In modern multiband and wideband radio frequency (RF) systems, good-performance tunable bandpass and bandstop filters have been extensively investigated for meeting the demands of multi-channel operation [1–6]. With the rapid development of innovative terahertz communication systems, terahertz filters are highly desired, which play an indispensable role in front end devices to select target frequency bands and reject undesired signals. In [7], a highpass filter is reported based on metamaterial with a "plasmonic" response to electromagnetic waves in the terahertz range. Additionally, using a microstrip line attached to photoconductive switches, a terahertz stopband frequency response is performed [8]. Then, a second-order bandpass terahertz filter is designed in [9] by multilayer complementary metamaterial structures. Based on band gaps properties, a lowpass filter by using metal slits in tapered parallel-plate waveguides is achieved [10]. However, these reported filters cannot implement the tunable frequency for multiband and wideband terahertz systems. For the tunable operation, the graphene-based tunable lowpass and bandpass filters are presented in the terahertz band, respectively [11, 12].

In this paper, we present a new graphene-based tunable bandstop filter at terahertz frequency band with a constant absolute bandwidth. To the best of the authors' knowledge, this work is the first tunable terahertz bandstop filter based on graphene materials. The proposed filter is composed of graphene-based three-section L resonators, conductor layers, and a SiO_2 substrate. The tuning frequency can be easily performed by only loading different chemical potentials on graphene surface. Therefore, the presented filter offers the following advantages: 1) tunable terahertz frequency band, 2) bandstop response for rejecting undesired signals, 3) constant absolute bandwidth, and 4) simple circuit model without any extra lossy devices and slotted ground structure.

Received 13 October 2017, Accepted 10 November 2017, Scheduled 25 November 2017

* Corresponding author: Mengdan Kong (kongmengdan001@gmail.com).

The authors are with the School of Electronic Engineering, Beijing Key Laboratory of Work Safety Intelligent Monitoring, Beijing University of Posts and Telecommunications, Beijing 100876, China.

2. THEORY AND ANALYSIS

2.1. *S*-Parameter Extraction for *L* Resonator

Figure 1(a) depicts the circuit configuration of the proposed bandstop filter based on three-section L resonators. In order to extract the S-parameters of the L resonators, a generalized two-port coupled line with a reactive element (X_T) and an open-circuit termination shown in Fig. 1(b) is analyzed and discussed. According to the mathematical results [13], the Z matrix elements of coupled-line section with port numbers definitions can be written as

$$\begin{cases} Z_{11}= Z_{22} = Z_{33} = Z_{44} = \dfrac{-j\left(Z_{oe}\cot\theta_e + Z_{oo}\cot\theta_o\right)}{2} \\ Z_{12}= Z_{21} = Z_{34} = Z_{43} = \dfrac{-j\left(Z_{oe}\cot\theta_e - Z_{oo}\cot\theta_o\right)}{2} \\ Z_{13}= Z_{31} = Z_{24} = Z_{42} = \dfrac{-j\left(Z_{oe}\csc\theta_e - Z_{oo}\csc\theta_o\right)}{2} \\ Z_{14}= Z_{41} = Z_{23} = Z_{32} = \dfrac{-j\left(Z_{oe}\csc\theta_e + Z_{oo}\csc\theta_o\right)}{2} \end{cases}, \tag{1}$$

where Z_{0e}, Z_{0o} and θ_e, θ_o denote the even-/odd-mode impedances and electrical length, respectively. Once port 2 is an open-circuit termination and port 3 connects a reactive element X_T, the Z matrix elements for ports I and O can be expressed as

$$Z_{II} = Z_{11} - \frac{Z_{13}^2}{Z_{11}+X_T}, \quad Z_{IO} = Z_{OI} = Z_{11} - \frac{Z_{13}Z_{34}}{Z_{11}+X_T}, \quad Z_{OO} = Z_{11} - \frac{Z_{34}^2}{Z_{11}+X_T}. \tag{2}$$

where ports 1 and 4 are redefined as ports I (Input) and O (Output) for convenience. Then, based on Eq. (2) the $ABCD$ matrix can be transformed form Z matrix as

$$\begin{cases} A = \dfrac{Z_{11}^2 + X_T Z_{11} - Z_{13}^2}{Z_{11}^2 + X_T Z_{11} - Z_{13}Z_{34}} \\ B = \dfrac{Z_{11}\left(Z_{13} - Z_{34}\right)^2}{Z_{11}^2 + X_T Z_{11} - Z_{13}Z_{34}} \end{cases}, \quad \begin{cases} C = \dfrac{Z_{11} + X_T}{Z_{11}^2 + X_T Z_{11} - Z_{13}Z_{34}} \\ D = \dfrac{Z_{11}^2 + X_T Z_{11} - Z_{34}^2}{Z_{11}^2 + X_T Z_{11} - Z_{13}Z_{34}} \end{cases}. \tag{3}$$

As shown in Fig. 1(b), an open-circuit stub is selected as the desired reactive element (X_T) in L resonator. Thus, it can be written as

$$X_T = -jZ_T\cot(\theta), \tag{4}$$

where Z_T represents the characteristic impedance of the open-circuit stub, and we assume that the electrical lengths of all the transmission lines are θ. By Eqs. (1), (3), and (4), the S-parameters can be

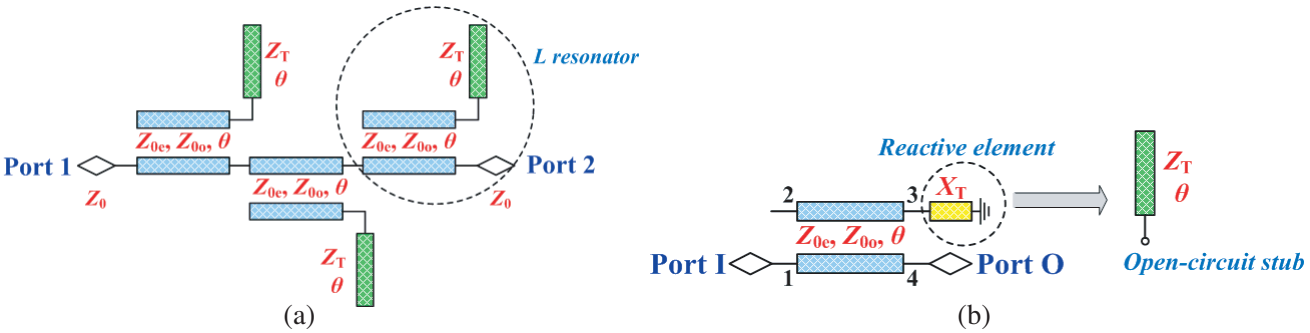

Figure 1. (a) The circuit configurations of the proposed bandstop filter. (b) The generalized two-port coupled line with a reactive element (X_T) and an open-circuit termination.

extracted as

$$S_{OI} = -\frac{4jZ_0\left[-Z_a^2 + Z_b(2Z_T + Z_b)\cos\theta\right]\cot\theta\csc\theta}{\left\{\begin{array}{l} -Z_a^2 Z_b\cot^3\theta + 2jZ_0Z_a^2\csc^2\theta - 2j\cot^2\theta\left[Z_0(2Z_b^2 - Z_a^2 + 4Z_TZ_b) + jZ_a^2Z_b\csc\theta\right] \\ +\cot\theta\left[4Z_0^2(2Z_T + Z_b) - Z_a^2Z_b\csc^2\theta\right] \end{array}\right\}}. \quad (5a)$$

and

$$\left\{\begin{array}{l} Z_a = Z_{0e} - Z_{0o} \\ Z_b = Z_{0e} + Z_{0o} \end{array}\right. . \quad (5b)$$

where Z_0 represents the port impedance of 50 Ω. In order to achieve the bandstop response, the S_{OI} should be equal to 0. Based on Eqs. (5a) and (5b), the electrical parameters of the proposed L resonator can be determined. Fig. 2(a) shows the ideal simulated results of the proposed bandstop filter composed of three-section L resonators with different electrical length θ. The even-/odd-impedances (Z_{0e}, Z_{0o}) and characteristic impedance (Z_T) of open-circuit stub are set as 80 Ω, 30 Ω, and 50 Ω, respectively. As shown in Fig. 2(a), the stopband frequency and bandwidth increases as the electrical length θ reduces and the insertion losses are less than −50 dB. In other words, the stopband frequency can be tuned by changing the electrical length θ. In addition, in order to determine the influence of the even-/odd-mode impedances and characteristic impedance of open-circuit stub on stopband bandwidth, we plot the relation between $|S_{11}|$ and Z_{0e}, Z_{0o}, Z_T using Advanced Design System (ADS) simulated software in Fig. 2(b). It is quite clear that the bandwidth of the proposed bandstop filter would be improved with the increasing of the coupling coefficient k [$k = (Z_{0e} - Z_{0o})/(Z_{0e} + Z_{0o})$], while the smaller Z_T can expand the stopband bandwidth.

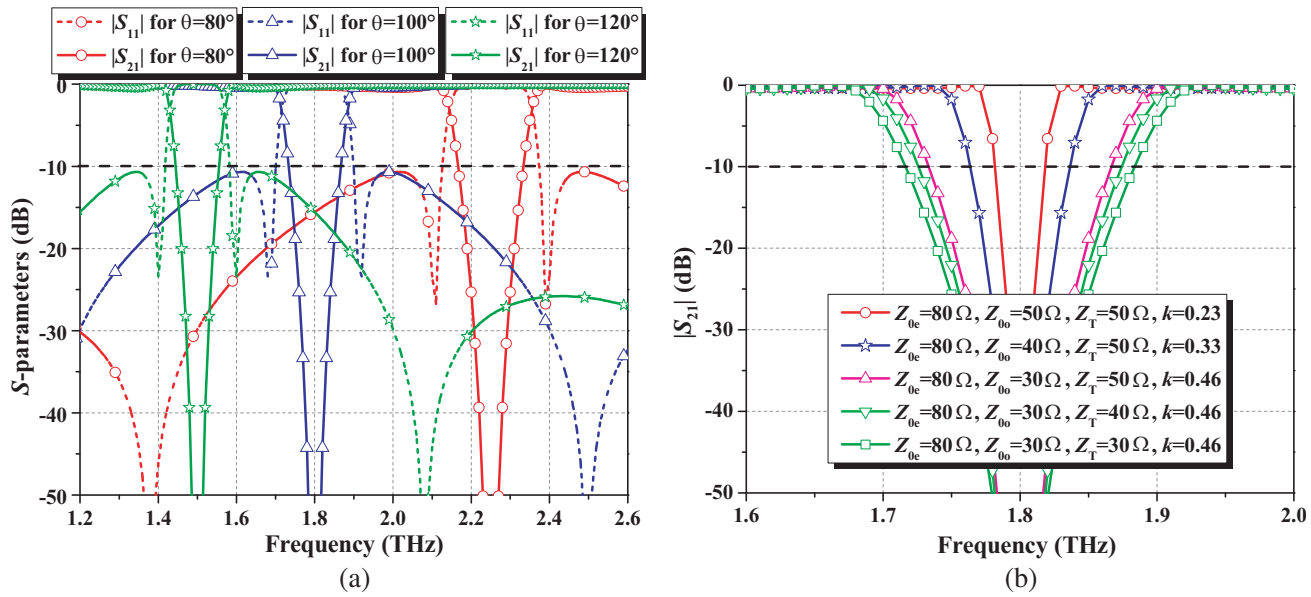

Figure 2. The ideal simulated results of the proposed bandstop filter composed of three-section L resonators with different (a) θ and (b) k, Z_T.

2.2. Graphene-based THz Tunable Bandstop Filter

The S-parameters and performance of the proposed bandstop filter have been discussed and analyzed. For extending to terahertz and tuning-frequency applications, in this paper we design a graphene-based tunable bandstop filter. Fig. 3 shows the proposed three-dimensional circuit model of tunable bandstop filter, which comprises graphene-based three-section L resonators, conductor layers, and a SiO_2 substrate. Note that in order to satisfy the manufacturing conditions of graphene including lyophobic property, good optical contrast, and high temperature resistance from 500 to 700°, the SiO_2 substrate

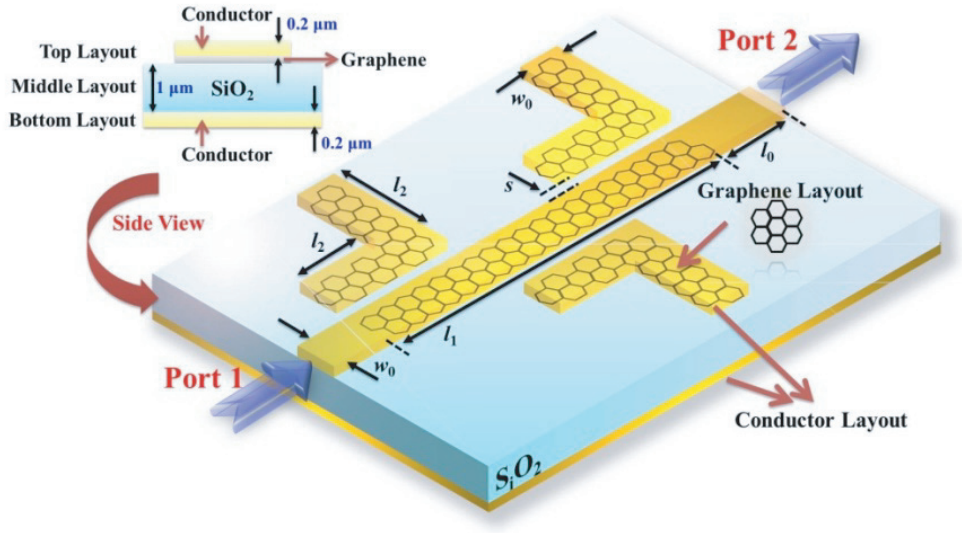

Figure 3. The three-dimensional model of the proposed tunable bandstop filter.

is utilized in this work. Based on Kubo's formalism, the graphene with frequency-dependent complex conductivity σ can be modeled as [14]

$$\sigma_{intra} \approx -j\frac{e^2 k_B T}{\pi\hbar^2(\omega - j\tau^{-1})}\left(\frac{\mu_c}{k_B T} + 2\ln\left(e^{-\mu_c/(k_B T)} + 1\right)\right), \tag{6a}$$

and

$$\sigma_{\text{inter}} \approx -j\frac{e^2}{4\pi\hbar}\ln\left(\frac{2\left|\mu_c\right| - \left(\omega - j\tau^{-1}\right)\hbar}{2\left|\mu_c\right| + \left(\omega - j\tau^{-1}\right)\hbar}\right), \tag{6b}$$

where e is the electron charge, k_B the Boltzmann's constant, τ the electron relaxation time in graphene, μ_c the chemical potential, $\hbar$ the reduced plank constant, ω the angular frequency, and T the temperature. It should be noted that only the intra-band conductivity σ_{intra} is considered in this work due to the slight influence of the inter-band conductivity σ_{inter}. As discussed above, the stopband frequency can be tuned by changing electrical length θ. Moreover, the conductivity σ of graphene can change the phase constant and surface impedance [11], which can be controlled by tuning chemical potential of graphene over a wide range typically from -1 to 1 eV from Eq. (6a). Accordingly, the graphene-based surface has a large potential to perform the tuning frequency via changing conductivity σ of graphene controlled by the chemical potential μ_c. Therefore, the surface impedance boundary can be used to establish the two-dimensional graphene model based on Equations (6a) and (6b) due to its property of an atom thickness In the real implementation, the chemical potential can be tuned over a typical range from 1 to 1 eV based on a transverse electric field using a dc-biased structure [11]. The approximate formula can be determined as

$$\mu_c \approx \hbar v_F \sqrt{\frac{\pi\varepsilon_r\varepsilon_0(V_{DC} - V_{Dirac})}{et}} \tag{7}$$

where V_{Dirac} is the voltage at the Dirac point, v_F ($\approx 10^6$) the Fermi velocity in graphene, and ε_r and t represent the permittivity and thickness of the gate dielectric, respectively.

3. RESULTS AND DISCUSSION

As shown in Fig. 3, the top and bottom layers of the proposed terahertz tunable bandstop filter are both perfect conductor with a thickness of 0.2 μm, while the middle layer is a SiO_2 substrate attached with graphene-based three-section L resonators. The SiO_2 substrate is with a dielectric constant of 3.8 and thickness of 1 μm. Finally, the full-wave electromagnetic simulation of the proposed terahertz

tunable bandstop filter is performed using HFSS software based on the finite element method (FEM). In this work, the initial conditions of $T = 300\,\mathrm{K}$ and $\tau = 1\,\mathrm{ps}$ are defined. Additionally, the physical dimensions depicted in Fig. 3 are determined as follows: $w_0 = 2\,\mu\mathrm{m}$, $s = 0.5\,\mu\mathrm{m}$, $l_0 = 10\,\mu\mathrm{m}$, $l_1 = 80\,\mu\mathrm{m}$, and $l_2 = 19.9\,\mu\mathrm{m}$. Note that in real implementations, the exited Van der Waals forces between graphene and substrate can make graphene layer adhere on the substrate very well. And the graphene can be clearly distinguished by optical microscope due to the good optical contrast of SiO_2 substrate.

Figure 4 plots the simulated results with different chemical potentials. The stopband frequencies are tuned at 1.605, 1.673, and 1.716 THz with the chemical potentials of 0.1, 0.3, and 1 eV. Moreover, the corresponding maximum attenuation levels are around 24.7, 25.7, and 29.3 dB, respectively, with 10-dB absolute bandwidth of 45, 40, and 46 GHz. In addition, the out-of-band insertion losses are always less than $-1\,\mathrm{dB}$, and they would reduce with the increasing of chemical potential The corresponding

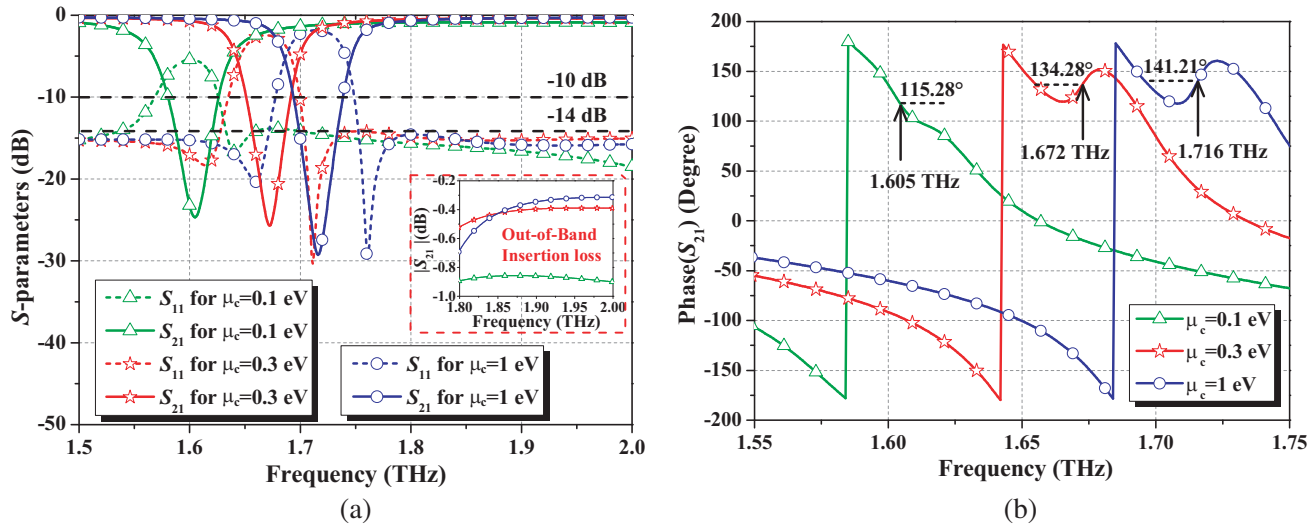

Figure 4. The full-wave electromagnetic simulated results of the proposed terahertz tunable bandstop filter with 0.1, 0.3, and 1 eV chemical potentials for (a) return loss ($|S_{11}|$) and insertion loss ($|S_{21}|$), and (b) phase response.

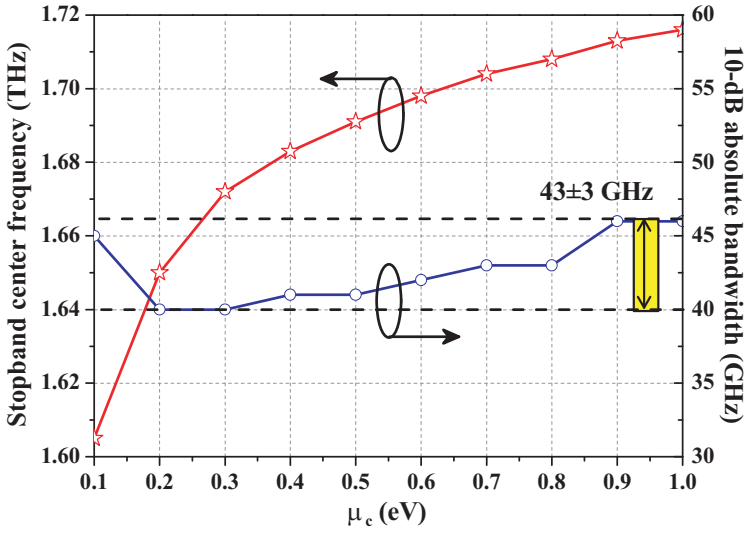

Figure 5. Stopband center frequency and 10-dB absolute bandwidth response versus chemical potentials μ_c.

phase responses are 115.28°, and 134.28°, and 141.21° at the stopband frequencies of 1.605, 1.673, and 1.716 THz. Besides, the out-of-band return loss is better than 14 dB. From Fig. 4, it can be seen that the stopband frequency, phase response, and attenuation level will improve as the chemical potential μ_c increases, while the level of out-of-band return loss has no obvious relation with μ_c.

In order to further determine the tunable frequency range of the proposed terahertz bandstop filter, we depict the relation between stopband center frequency, 10-dB absolute bandwidth and chemical potentials in Fig. 5. All data are obtained based on the HFSS software by sweeping the different chemical potentials from 0.1 to 1 eV with a step length of 0.1 eV. As shown in Fig. 5, the stopband center frequency increases with the increasing of μ_c, while the absolute bandwidth varies weakly. Accordingly, in the case of $0 < \mu_c \leq 1$ eV and in-band $|S_{21}| < -10$ dB, the tunable frequency range of the proposed bandstop filter is from 1.6 to 1.72 THz with a constant absolute bandwidth of 43 ± 3 GHz. Therefore, a terahertz reflective tunable bandstop filter with a constant absolute bandwidth can be established based on the designed graphene-based L resonators.

4. CONCLUSIONS

In this paper, a novel terahertz tunable bandstop filter with constant absolute bandwidth is designed and discussed by using graphene-based three-section L resonators, conductor layers, and a SiO_2 substrate. Both theoretical predictions and simulated verifications show that the stopband frequency can be tuned by changing the chemical potentials. Apart from major advantages of tunable terahertz stopband frequency band with constant absolute bandwidth, the proposed bandstop filter provides a good out-of-band return loss, high in-band attenuation level, and simple circuit model without any extra lossy devices and slotted ground structure. Therefore, it can be expected that this bandstop filter will be extensively applied in the innovative terahertz communication systems for rejecting undesired signals.

ACKNOWLEDGMENT

This work was supported in part by the National Natural Science Foundations of China (No. 61327806, No. 61422103, and No. 61671084), and National Key Basic Research Program of China (973 Program) (No. 2014CB339900).

REFERENCES

1. Zhang, X. Y., C. H. Chan, Q. Xue, and B.-J. Hu, "RF tunable bandstop filters with constant bandwidth based on a doublet configuration," *IEEE Trans. Ind. Electron.*, Vol. 59, 1257–1265, 2012.
2. Chen, J.-X., J. Shi, Z.-H. Bao, and Q. Xue, "Tunable and switchable bandpass filters using slot-line resonators," *Progress In Electromagnetics Research*, Vol. 111, 25–41, 2011.
3. Saeedi, S., J. Lee, and H. H. Sigmarsson, "Novel coupling matrix synthesis for single-layer substrate-integrated evanescent-mode cavity tunable bandstop filter design," *IEEE Trans. Microw. Theory Techn.*, Vol. 63, 3929–3938, 2015.
4. Jeong, S. and J. Lee, "Frequency- and bandwidth-tunable bandstop filter containing variable coupling between transmission line and resonator," *IEEE Trans. Microw. Theory Techn.*, Vol. PP, No. 99, 1–11, 2017.
5. Guyette, A. C., E. J. Naglich, and S. Shin, "RF-power-activated and signal-tracking tunable band-stop filters," *IEEE Trans. Microw. Theory Techn.* Vol. 65, 1534–1544, 2017.
6. Esmaeili, M. and J. Bornemann, "Novel tunable bandstop resonators in SIW technology and their application to a dual-bandstop filter with one tunable stopband," *IEEE Microw. Compon. Lett.*, Vol. 27, 40–42, 2017.
7. Wu, D., N. Fang, C. Sun, X. Zhang, W. J. Padilla, D. N. Basov, D. R. Smith, and S. Schultz, "Terahertz plasmonic high pass filter," *Appl. Phys. Lett.*, Vol. 83, 201–203, 2003.
8. Cunningham, J., C. Wood, A. G. Davies, I. Hunter, H. E. Linfield, and E. H. Beere, "Terahertz frequency range band-stop filters," *Appl. Phys. Lett.*, Vol. 86, 213503, 2005.

9. Lu, M., W. Li, and E. R. Brown, "Second-order bandpass terahertz filter achieved by multilayer complementary metamaterial structures," *Opt. Lett.*, Vol. 36, 1071–1073, 2011.
10. Lee, E. S., S.-G. Lee, C.-S. Kee, and T.-I. Jeon, "Terahertz notch and low-pass filters based on band gaps properties by using metal slits in tapered parallel-plate waveguides," *Opt. Exp.*, Vol. 19, 14852–14859, 2011.
11. Perruisseau-Carrier, J. and A. Álvarez-Melcón, "Graphene-based plasmonic tunable low-pass filters in the terahertz band," *IEEE Trans. Nanotechnol.*, Vol. 13, 1145–1153, 2014.
12. Yao, Y., X. Cheng, S.-W. Qu, J. Yu, and X. Chen, "Graphene-metal based tunable band-pass filters in the terahertz band," *IET Microw. Antennas Propag.*, Vol. 10, 1570–1575, 2016.
13. Pozar, D. M., *Microwave Engineering*, 3rd Edition, Publishing House of Electronics Industry, 2006.
14. Hanson, G. W., "Dyadic Green's functions and guided surface waves for a surface conductivity model of graphene," *J. Appl. Phys.*, Vol. 103, 064302, 2008.